

pubs.acs.org/JPCL Letter

# Regulation of Oxygen Redox in Disordered Rock-Salt LiXO<sub>2</sub> Li-Ion Cathodes by Cation Effects: A First-Principles Study

Yanzhao Niu, Shisheng Wang, Ruishan Zhang, Zengzhu Li, Feng Pan, Wei Deng, and Bingkai Zhang\*



Cite This: J. Phys. Chem. Lett. 2025, 16, 8105-8113



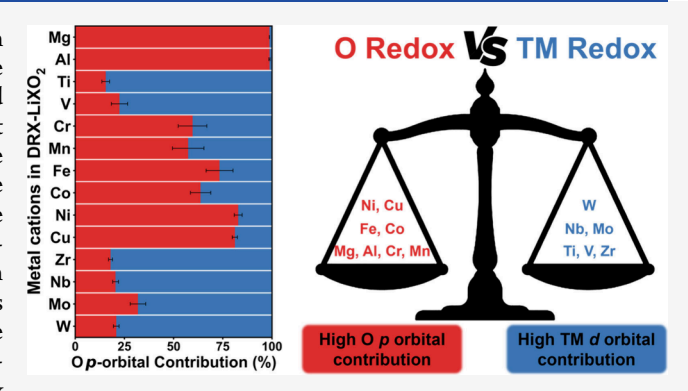
**ACCESS** I

III Metrics & More

Article Recommendations

Supporting Information

ABSTRACT: The modulation of anionic redox reactions has been demonstrated to significantly enhance the performance of oxide cathode materials. To elucidate this phenomenon, we conducted comprehensive first-principles calculations on disordered rock-salt (DRX) cathode materials with simple stoichiometry, which have emerged as highly promising candidates due to their unique structural and compositional flexibility. Our comprehensive investigation combining qualitative evaluation of oxygen coordination environment, quantitative analysis of metal—oxygen electronic states, and systematic magnetic characterization reveals two anion redox mechanisms in DRX: the reversible reductive coupling mechanism and irreversible oxygen dimerization mechanism. A three-tier framework for categorizing cation redox



behavior is established based on the extent of anion redox contribution: Cu and Ni strongly promote oxygen redox; Cr, Mn, Fe, and Co show moderate participation; while Ti, V, Zr, Nb, Mo, and W exhibit minimal involvement. Furthermore, by studying systems doped with multiple cations, we demonstrated that cationic effects could regulate oxygen redox behavior. These insights provide valuable guidance for the rational design of DRX cathode materials with enhanced performance and durability.

ithium-ion batteries, the backbone of modern energy ✓ storage, power applications ranging from portable electronics to electric vehicles and grid-scale storage. Advances in their energy density primarily rely on breakthroughs in the development of cathode materials. 1,2 Recently, disordered rock-salt LiMnO2 (DRX-LMO) materials have garnered considerable research attention owing to their inherent cationic disorder, which facilitates unique structural flexibility and superior electrochemical performance.<sup>3</sup> In conventional cathode materials, transition metals are typically considered the primary source of electrochemical activity, with the capacity corresponding to the number of electrons that can be exchanged per unit mass of the transition metal.<sup>4</sup> In contrast, DRX-LMO features Li-O-Li configurations that effectively activates oxygen redox activity, leading to distinct voltage profiles and phase transitions, thereby enabling higher capacity. 5,6 However, the local oxygen configuration that supports redox activity is not always maintained during the dynamic intercalation processes, potentially leading to the formation of O-O dimers or even O2 evolution. Substantial evidence of structural transitions around oxygen after electrochemical cycling has been reported in numerous experimental studies. Compared to systems lacking anionic redox, the involvement of oxygen in redox reactions introduces unstable O 2p states and oxygen holes may promote the formation of O–O dimers or even  $O_2$  evolution, thereby undermining the cycling stability of the structure. Therefore, cycling stability

in systems with anionic activity has long been a debated topic in this field. In DRX materials, it is essential to prevent structural damage caused by excessive oxygen participation while preserving structural integrity and maximizing the capacity gains afforded by anion redox activity.

To optimize oxygen redox activity in DRX materials, a variety of strategies have recently been proposed. Ceder et al. demonstrated that multication doping can be achieved in DRX cathode materials. Their work revealed an inverse correlation between transition metal (TM) cation diversity and shortrange order, accompanied by consistent increases in energy density and rate performance. Zhou et al. investigated a series of  $x \text{Li}_2 \text{TiO}_3$ - $(1-x) \text{LiMnO}_2$  ( $0 \le x \le 1$ ) materials by varying the metal cation content in Li-rich DRX. Their results demonstrated that adjusting both the proportion and quantity of metal cations can effectively modulate the activity and extent of oxygen redox, thereby enhancing cycling stability. Recent studies confirm the  $\text{Li}_{4+x} \text{MoO}_5 \text{F}_x$  fluorinated rock-salt system uniquely combines TM-O hybridization and fluorine-

Received: May 21, 2025 Revised: July 27, 2025 Accepted: July 29, 2025 Published: August 1, 2025





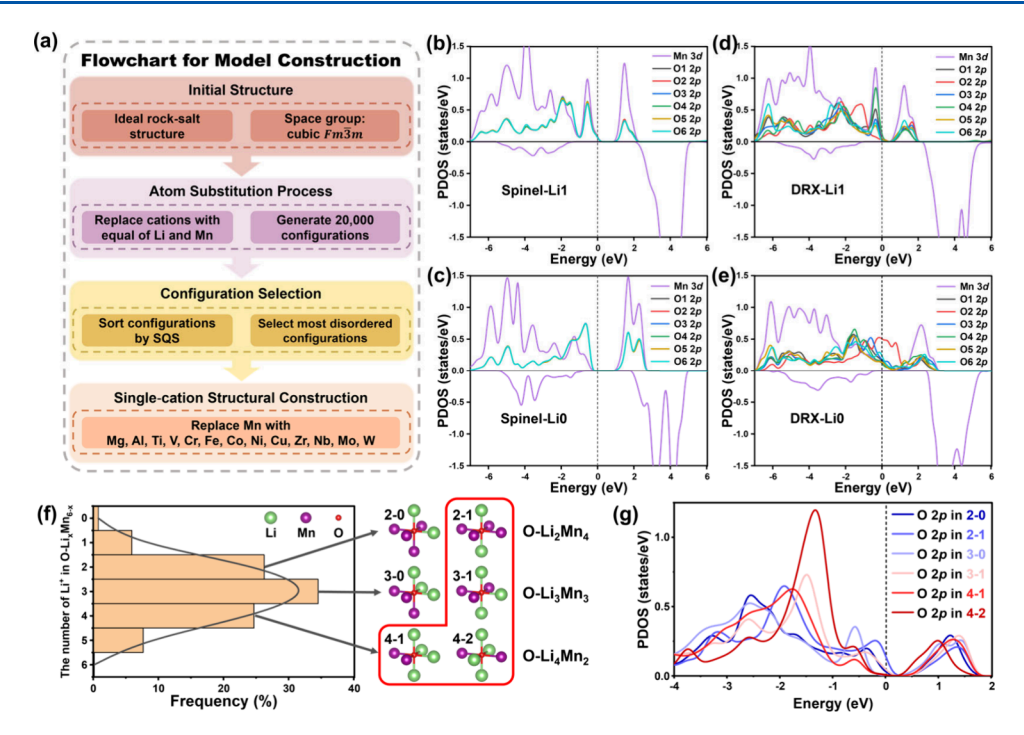


Figure 1. (a) Workflow for constructing the DRX-LMO crystal structure. (b–e) PDOS of the Mn 3d and O 2p orbitals within the MnO<sub>6</sub> octahedral units in the Li1 and Li0 states. The DRX structure shown is the lowest-energy configuration selected from 20 DRX-LMO models. (f) Statistical distribution of oxygen first shell environment in the DRX-LMO. (g) The corresponding PDOS of an O 2p orbital for the structural units displayed in (f).

regulated anionic redox to achieve 438 mAh/g capacity while inhibiting oxygen loss, resolving a fundamental challenge in oxygen-redox cathodes. <sup>13</sup> Although numerous studies have advanced breakthroughs in the redox mechanisms and anionic activity of DRX materials, <sup>6,14–16</sup> successful commercial applications have yet to be realized. These promising materials could gain a competitive edge in the future due to the capacity enhancements enabled by anionic activity. While various modification strategies, including doping, have been explored in DRX frameworks, there is still a lack of systematic studies summarizing the effects of different cationic elements, particularly quantitative methods for evaluating anionic activity.

In this study, we systematically and successfully constructed ideal DRX structural models and employed first-principles calculations to investigate the structural and electronic characteristics of various metal cations within the DRX framework, thereby elucidating the intrinsic relationship between Li-O-Li configurations and oxygen redox activity. Furthermore, we conducted an in-depth analysis of oxygen participation in redox reactions within the DRX system, introducing two mechanistic models, the reversible reductive coupling mechanism (RCM) and the irreversible oxygen dimerization mechanism (ODM), to explain different degrees of oxygen involvement. We also proposed a novel quantitative descriptor, the O p-orbital contribution, to serve as a metric for the extent of oxygen redox participation. Additionally, we attempted and successfully employed multications doping to tune oxygen anion redox behavior. This work provides a theoretical foundation and innovative strategies for designing high-capacity, long-lifetime, and high-performance DRX manganese-based cathode materials, thereby advancing the practical application of next-generation lithium-ion battery technologies.

The cation disorder inherent to DRX materials introduces unavoidable potential errors into computational analyses. To mitigate these errors, we employed the model-building workflow illustrated in Figure 1(a), with detailed procedures and model validation described in the Supporting Information. Importantly, we retained 20 base models for our statistical calculations. Although this strategy generates a substantial computational workload and requires significant resources, it effectively enhances the reliability of our results while minimizing the influence of potential errors.

To investigate the oxygen redox behavior in DRX materials, we first compared a Mn-based DRX phase with the spinel LiMn<sub>2</sub>O<sub>4</sub> (spinel-LMO) to analyze how differences in geometric structure influence their electronic structures, as shown in Figure 1b-e. The projected density of states (PDOS) for oxygen shows that the six O 2p orbitals surrounding Mn in spinel-LMO overlap almost completely in both the fully lithiated (Li1) and the fully delithiated (Li0) states as a result of the ordered cationic structure. 17 In the Li1 state, the Mn 3d and O 2p orbitals are hybridized near the Fermi level. Upon delithiation to the Li0 state, the Mn 3d orbital vanishes, and the antibonding states become more pronounced, indicating a progressive oxidation of Mn from a lower to a higher valence state. Meanwhile, the distribution and intensity of the O 2p orbitals near the Fermi level change very little, suggesting that oxygen contributes minimally to the electron transfer process and that the overall redox reaction is predominantly governed by the Mn 3d orbitals. In contrast, the six O 2p PDOS in DRX-LMO exhibit distinct energy distributions in both the Li1 and Li0 states, due to cation disorder. After delithiation to the Li0 state, the Mn 3d peak disappears, and the intensity of the O 2p peak is also significantly reduced. Notably, the PDOS of the O2 2p orbitals (Figure 1d,e) differs markedly from that of other oxygen

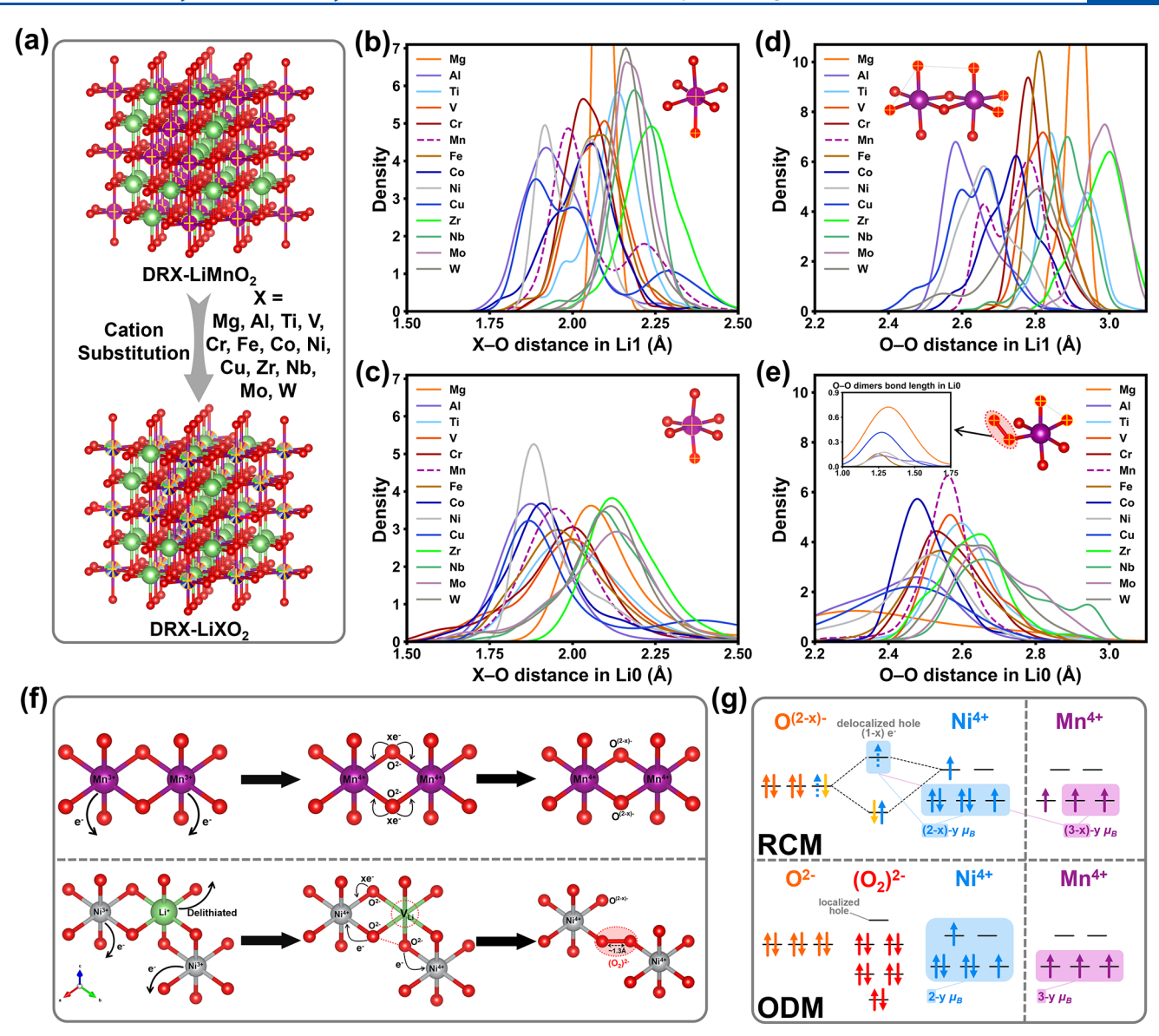


Figure 2. (a) Single-cation DRX-LMO derivatives were modeled through complete Mn substitution. Green spheres represent Li, purple spheres represent Mn, red spheres represent O, and multicolored spheres represent various metal cations. (b–e) The distributions of X–O and O–O distances before and after delithiation in single-cation structures with different cations. The inset in (e) shows the O–O distance distributions at dimer formation. (f) Schematic illustration of the mechanisms by which varying degrees of oxygen participation during delithiation lead to X–O bond shortening and O–O dimer formation. (g) Schematic illustration of TM–O orbital hybridization and magnetic moment differences with and without O–O dimer formation.

atoms, a distinction that arises from its unique local Li-O-Li environment. In the Li1 state, it does not hybridize with Mn 3d orbitals, whereas in the Li0 state its O 2p peak shifts above the Fermi level, exhibiting pronounced hole-like features. <sup>9,10</sup> These hole states will supply charge compensation to the transitionmetal centers. This provides strong evidence for oxygen's participation in the redox process.

Given the substantial differences in the electronic structures of the equivalent  $\mathrm{MnO_6}$  octahedral units in spinel-LMO and DRX-LMO, which are intimately tied to the unique structural features of the DRX materials, it is necessary to investigate the local geometric environments and electronic states of oxygen in DRX-LMO. We analyzed the first shell environment around oxygen by statistically quantifying the occupancy frequency corresponding to different lithium contents (x values) of the O-Li $_x$ Mn $_{6-x}$  octahedra across all structures. The results, as

depicted in Figure 1f, indicate that the highest frequency occurs at x = 3 and that the overall distribution approximates a normal distribution, thereby aligning with our model expectations and confirming the successful construction of an ideal DRX material via our quasi-random method. When x = 2, 3, or 4, the structural units exhibit distinct oxygen coordination environments. In the Figure 1f, the schematic diagrams of the O-Li<sub>2</sub>Mn<sub>4</sub>, O-Li<sub>3</sub>Mn<sub>3</sub>, and O-Li<sub>4</sub>Mn<sub>2</sub> octahedral units are displayed in the right panel sequentially from top to bottom. Each octahedron is designated using the "x-y" format, where xindicates the number of Li atoms in O-Li<sub>x</sub>Mn<sub>6-x</sub> and y denotes the number of Li-O-Li configurations within that octahedron. The structures highlighted by red boxes are octahedral with linear Li-O-Li configurations, and it is precisely the presence of these configurations that activates oxygen redox.<sup>6,18</sup> Moreover, the proportion of Li-O-Li

configurations within the octahedral units also influences oxygen redox behavior. Accordingly, we analyzed the PDOS of the O 2p orbitals for the six different oxygen coordination environments presented in Figure 1f. The results, illustrated in Figure 1g, illustrate a color gradient that shifts from blue to red as the number of Li<sup>+</sup> and Li–O–Li increases within the octahedral units, indicating that the overall O 2p orbital distribution moves closer to the Fermi level and that oxygen redox activity is progressively enhanced. <sup>19,20</sup> Consequently, a higher proportion of Li–O–Li configurations correlates with an increased likelihood of oxygen atoms participating in redox reactions. <sup>21,22</sup> Although oxygen redox imparts additional electrochemical activity to the material, it may concurrently present challenges regarding structural stability, which will be discussed in the subsequent content.

The next question is whether other cation systems of DRX phases exhibit distinct redox behavior and structural stability during delithiation. To address this, we present a systematic investigation into the effects of different metal cations on the regulation of oxygen redox behavior and structural stability in DRX-LMO, as shown in Figure 2a. In physical research, simple and clean models are the best samples for studying individual factors. Therefore, we completely substituted Mn in DRX-LMO with various metal cations, resulting in a series of singlecation structural models (LiXO<sub>2</sub>, X = Mg, Al, Ti, V, Cr, Fe, Co, Ni, Cu, Zr, Nb, Mo, W). Although elements such as Mg, Al, and Ti may exhibit limited electrochemical activity, previous work has demonstrated their effectiveness as dopants for modulating the electrochemical behavior and stability of cathode materials. 12,23-25 Likewise, the use of Co and Nb in small concentrations can adjust material performance while largely alleviating sustainability-related application constraints. 14,26 Our study serves as a theoretical exploration aimed at clarifying the mechanistic roles of various metal cations in regulating oxygen activity. Consequently, it is important to adopt a broad research scope to inform the design and optimization of future DRX materials. It should be noted that the pure Al- and Mg-based structures are used here merely as reference mode ls to study pure oxygen redox behavior. Such idealized oxygen oxidation may not occur in practice, as it is likely accompanied by a series of phase transformation processes.

In order to assess the structural stability of these 14 singlecation structures DRX-LXO, we analyzed the distributions of X-O and O-O distances in both the Li1 and Li0 states, and the results are shown in Figure 2b-e, with corresponding statistical plots provided in Figure S3. Based on the graphical data, the Li0 state exhibits shorter distance of X-O and a more concentrated distance distribution than the Li1 state. We analyzed the microscopic mechanism underlying this phenomenon (Figure 2f). During delithiation, Mn3+ is oxidized to higher-valent  $Mn^{4+}$ , driving  $O^{2-}$  to compensate the charge via the Mn-O bonds and form  $O^{-(2-x)}$  with delocalized holes.<sup>27–29</sup> The migration of oxygen electrons enhances the localized electron density in the Mn-O bonds, strengthening covalency and further shortening the bond lengths.<sup>30</sup> Additionally, in the Li1 state, the Mn-O bonds exhibit a pronounced Jahn–Teller distortion, as previously reported in the literature, <sup>31,32</sup> thereby corroborating the reliability of our model. Furthermore, the structures corresponding to Ni and Cu also display uneven bond length distributions, indicating possible distortion in their respective octahedral environments. In addition, the X-O bond lengths in the structures

corresponding to the fifth-period elements Zr, Nb, and Mo, as well as the sixth-period element W, are noticeably longer than those observed for the other elements; their corresponding structural volumes are also larger (Figure S4), which is likely attributed to their relatively larger atomic radii.

Because the formation of O-O dimers negatively impact the cycling stability of the DRX material, we performed statistical analyses of the O-O distance distributions in our models. Data presented in Figure 2b-e and S3 reveal that in the Li0 state the distances of O-O are markedly reduced, which directly corresponds to the reduction in structural volume following delithiation. Moreover, the inset in Figure 2e indicate that in the Li0 state, structures containing Mg, Al, Fe, Ni, and Cu exhibit short O-O distance with an average length of approximately 1.3 Å, which is close to the length of the O-O bonds characteristic of O<sub>2</sub> molecules (1.2 Å). Previous studies have reported that systems with extensive oxygen redox can evolve  $O_2$  in the delithiated state.<sup>7–9</sup> To probe this possibility, we calculated the oxygen vacancy formation energies for our DRX-LiXO<sub>2</sub> models.<sup>33</sup> As shown in Figure S5, the oxygen vacancy formation energies vary significantly across different metal cation systems. In particular, systems prone to O-O dimer formation exhibit lower vacancy formation energies than others. From a thermodynamic perspective, these systems are more likely to form O-O dimers or oxygen vacancies under deep delithiation, which increases the risk of oxygen loss and adversely affects structural stability. By examining the structures in which O-O dimers form, we readily observe that these dimers predominantly appear adjacent to lithium vacancies (V<sub>Li</sub>). From a spatial perspective, Li<sup>+</sup> extraction and migration create V<sub>Li</sub> sites, which in turn grant nearby oxygen ions greater spatial freedom and enable O-O dimers formation. We explain the oxygen electron-transfer behavior during O-O dimers formation (Figure 2f) by analyzing a representative DRX-LiNiO<sub>2</sub> system that exhibits clear O-O dimers formation. During delithiation, Li+ migration generates V<sub>Li</sub>, and Ni<sup>3+</sup> is oxidized to Ni<sup>4+</sup>. Simultaneously, electrons from O<sup>2-</sup> near the V<sub>Li</sub> transfer: the electrons transferred into the Ni-O bonds cause their bond lengths to shorten; those that migrate onto the Ni<sup>4+</sup> centers provide charge compensation, potentially enabling continued redox participation and contributing to the high capacity; 29 and the oxygen ions that undergo electron transfer also hybridize their orbitals with those of neighboring oxygen ions, leading to the formation of O-O dimers.<sup>30</sup> Notably, the Ni-O bond functions like an electronic reservoir: accepting, storing, and redistributing electrons, and thus provides a pathway for oxygen electron transport in DRX systems.

When analyzing transition-metal magnetic moments, we observed that metals adjacent to O–O dimers exhibit significantly higher moments than those situated farther from the dimers (see Table S2 for the statistical data). We explain this phenomenon using the mechanism illustrated in Figure 2g, providing insight into the link between enhanced transition-metal magnetic moments and O–O dimer formation. In the Li0 state of DRX-LiNiO<sub>2</sub>, Ni<sup>4+</sup> adopt a d orbital configuration of  $t_{2g}^{\ 5}e_{g}^{\ 1}$ , which ideally corresponds to a net magnetic moment of approximately 2.0  $\mu_{B}$ . However, our calculations yield an average Ni<sup>4+</sup> moment of only 0.98  $\mu_{B}$ . We attribute this reduction to the RCM. During charging, O<sup>2-</sup> anions compensate the transition-metal charge and convert into O<sup>(2-x)<sup>-</sup></sup> carrying x oxygen holes. These hole-bearing electron

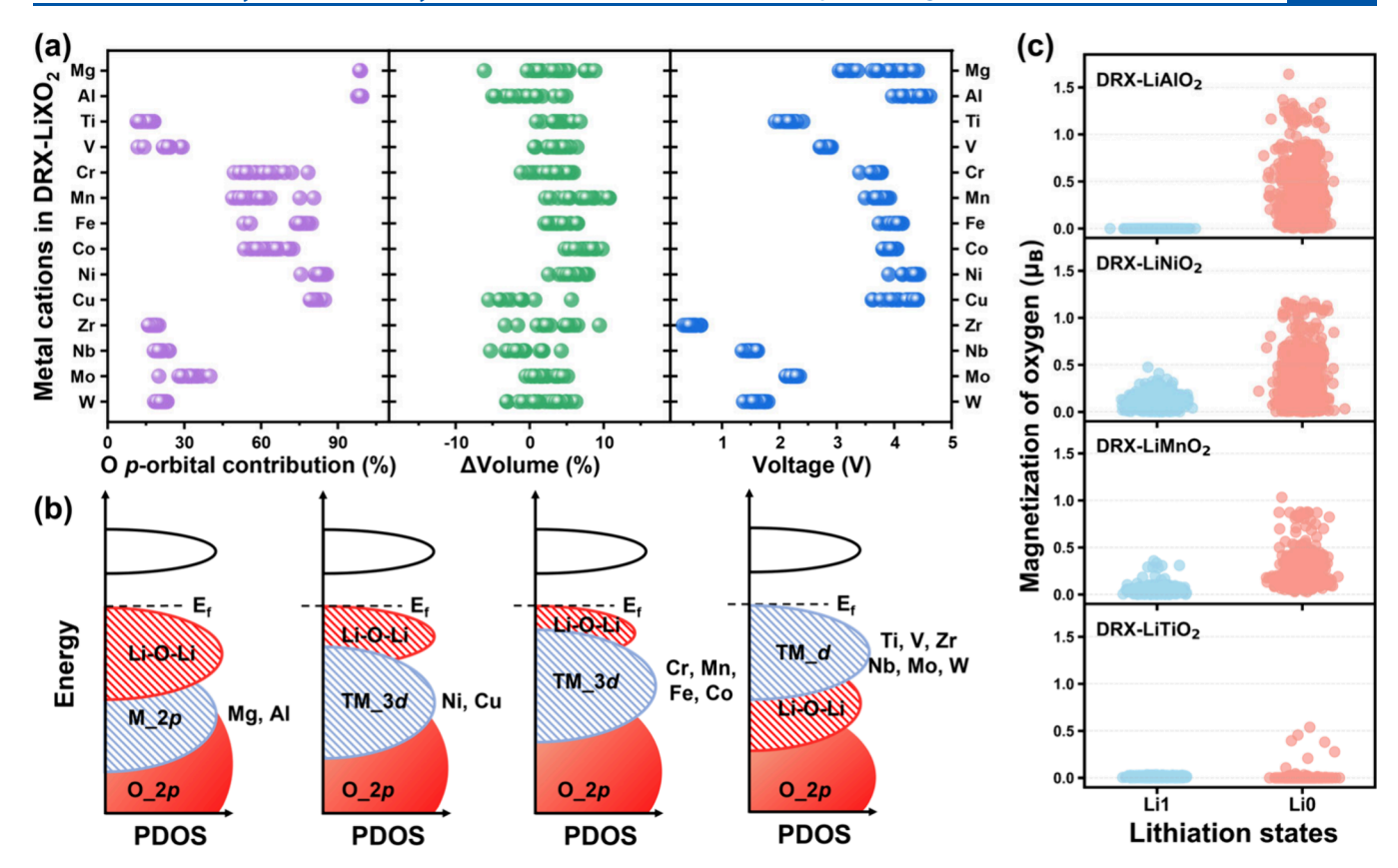


**Figure 3.** (a) O *p*-orbital contribution, volume change, and voltage corresponding to different metal cations. (b) Schematic illustration of M 3*d* and O 2*p* PDOS distributions for different levels of O *p*-orbital contribution, arranged from left to right in decreasing order of O *p*-orbital contribution. (c) Distribution of oxygen magnetic moments for representative structures selected from the four O *p*-orbital contribution categories (see Figure S6 for the distributions in all single-cation structures).

pairs hybridize with the single  $e_{\rm g}$  electron of Ni<sup>4+</sup> to form  $\sigma$ bonding electron pairs and  $\sigma^*$  delocalized holes totaling (1 –  $(x)e^{-34}$  The  $\sigma^*$  electrons together with the remaining unhybridized Ni<sup>4+</sup> electrons yield a total magnetic moment of  $(2 - x) \mu_B$ . Introducing a correction factor y to account for the influence of the other oxygen electrons in the NiO6 unit yields a total magnetic moment of  $((2 - x) - y) \mu_{R}$ , which explains the lower observed moment. In contrast, we observe that NiO<sub>6</sub> units exhibiting O-O dimers show a higher Ni<sup>4+</sup> moment ( $\sim$ 1.50  $\mu_{\rm B}$ ) than those without dimers. To explain this, we propose the ODM. For  $O^{2-}$  anions near  $V_{\rm Li}$  that undergo more charge compensation, those lacking oxygen holes and behaving as O-, the p orbitals of two adjacent Ospecies hybridize to form an  $(O_2)^{2-}$  unit, comprising five bonding electron pairs and one localized hole. Because the unpaired electrons on Ni4+ do not hybridize with oxygen in this scenario, the total magnetic moment becomes  $(2 - y) \mu_{B}$ an increase of  $x \mu_B$  relative to the RCM case, accounting for the higher moment.<sup>35</sup> We have similarly constructed orbital hybridization diagrams and estimated the magnetic moments for Mn<sup>4+</sup> in DRX-LiMnO<sub>2</sub>. However, in that system, the RCMdriven anionic charge compensation mechanism predominates, and ODM-driven O-O dimers formation is not apparent. Thus, in DRX materials with varying degrees of anionic redox activity, RCM and ODM operate in competition.

Different metal cation systems exhibit varying dominance of the RCM versus the ODM in their anionic chargecompensation processes, leading to distinct degrees of oxygen participation in redox reactions. In this study, we propose a

novel metric, the O p-orbital contribution, as a key criterion for quantitatively assessing the influence of various elements on oxygen redox behavior. The calculation method for this descriptor is detailed in the Supporting Information (Equation S2). Since the O p-orbital contribution directly reflects the electronic structure, it serves as a simple and broadly applicable electronic descriptor for the other system where oxygen participates in redox activity. As shown in Figure 3a, we plotted the O p-orbital contribution for various cations. The higher the proportion of O 2p states, the greater the O p-orbital contribution. Based on the calculated O p-orbital contributions, the metal cations can be classified into the following categories: (1) Mg and Al exhibit contributions approaching 100%; (2) Ni and Cu are about 80%; (3) Cr, Mn, Fe, and Co are around 60%; and (4) Ti, V, Zr, Nb, Mo, and W show values of approximately 20%. In Figure 3b, we present schematic PDOS plots for these four cases, where orbitals closer to the Fermi level are more readily active during redox reactions. We further examined each cation system's voltage, volume change, and O p-band center, as shown in Figures 3a and S6 (calculation details are provided in Equations S3-S6). We observed a clear correlation between the O p-orbital contribution and the O p-band center: as the O p-orbital contribution increases, both the voltage and the O p-band center also increase, and vice versa. This relationship arises because the O p-band center, which represents the average energy level of the O 2p orbitals relative to the Fermi level, increases as the oxygen atoms become more prone to electron loss during redox processes.<sup>36</sup> However, the O p-band center

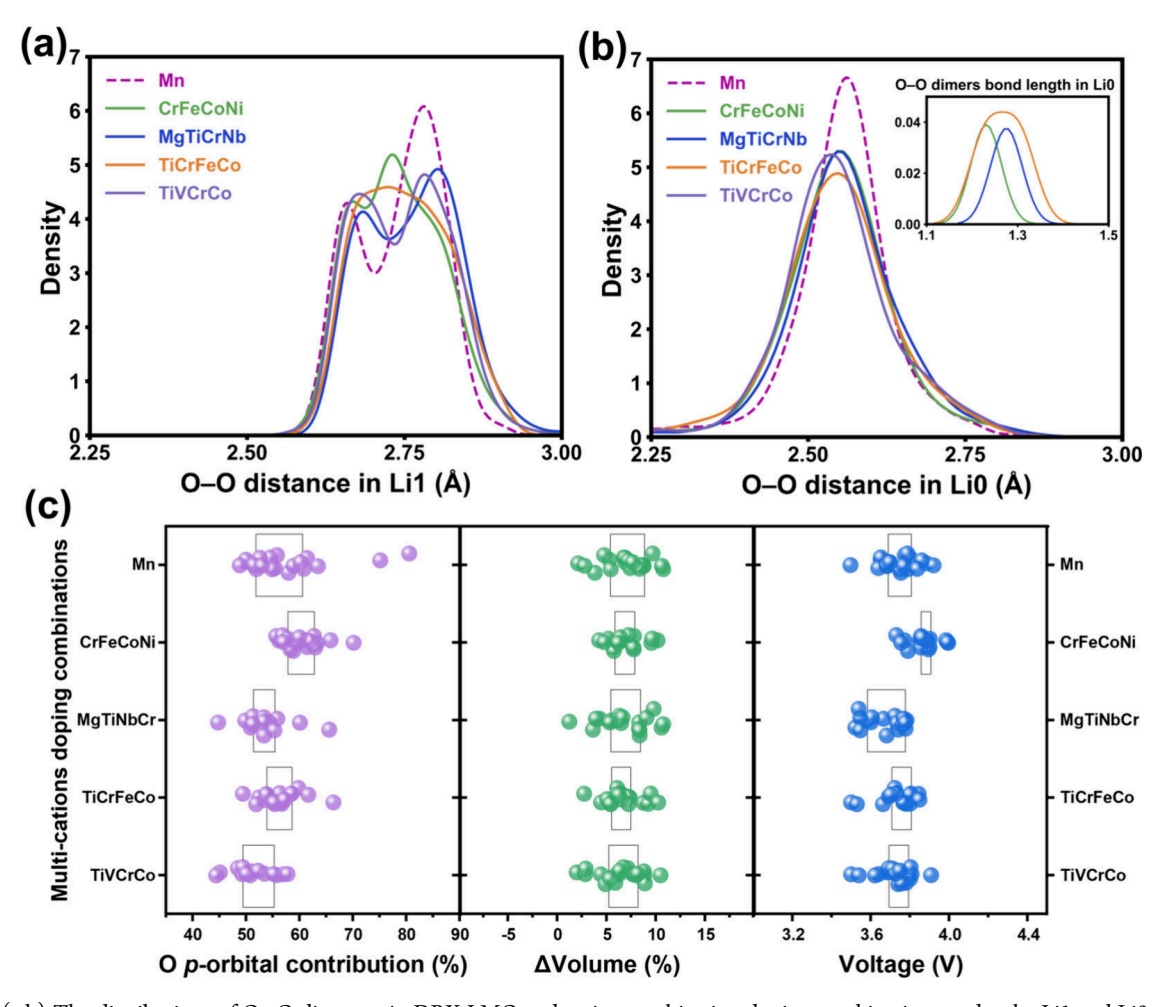


**Figure 4.** (a,b) The distributions of O–O distances in DRX-LMO and various multication doping combinations under the Li1 and Li0 states. The inset in (b) shows the O–O distance distributions at dimer formation. The doping combinations correspond to CrFeCoNi, MgTiCrNb, TiCrFeCo, and TiVCrCo, along with undoped LiMnO<sub>2</sub>. (c) Box plots of the O *p*-orbital contribution, volume change, and voltage for DRX-LMO with various multication doping combinations (the box represents the interquartile range from 25% to 75%).

accounts only for the absolute PDOS of oxygen without considering its energy alignment with the transition-metal states, thus our new descriptor offers a more suitable and intuitive measure for comparing energy relationships between transition metals and oxygen. Consequently, in DRX materials, oxygen is more inclined to participate in redox reactions when its O p-orbital contribution is higher. Furthermore, we found that the trend in oxygen vacancy formation energies shown in Figure S5 aligns with the *p*-orbital contribution data: systems with higher p-orbital contributions generally exhibit lower oxygen vacancy formation energies. Consequently, materials with high oxygen redox activity tend to display poorer lattice oxygen stability under deep delithiation. This observation further highlights the importance of regulating oxygen redox in order to optimize the stability of DRX materials. We also observed that structures containing Mg and Al exhibit an O porbital contribution approaching 100% along with correspondingly high voltages. This is attributed to the fact that the metal cations in these systems provide virtually no electrochemical activity during the redox process, leaving oxygen as the sole active contributor. Moreover, because oxygen electrons encounter a high energy barrier for migration, these structures exhibit elevated voltages. 23 In contrast, metal cations such as Ti, V, Zr, Nb, Mo, and W, which have relatively abundant vacant d orbitals, exhibit strong hybridization with O 2p

electrons, leading to robust X-O bonding. This strong bonding diminishes the local electronic environment of oxygen in the Li-O-Li configuration, resulting in lower overall O porbital contributions and voltage. Conversely, Ni and Cu, with fewer vacant d orbitals and weaker X-O hybridization, allow oxygen electrons more opportunities to participate in redox reactions, thereby yielding higher O p-orbital contributions. Elements like Cr, Mn, Fe, and Co display intermediate numbers of vacant d orbitals, corresponding to moderate O porbital contributions. In addition to using the O p-orbital contribution to quantify oxygen redox activity, we also performed statistical analyses of changes in oxygen magnetic moments to provide an intuitive measure of oxygen participation across different cation systems.<sup>33</sup> The four scatter plots in Figure 3c, corresponding to one of the four contribution levels, clearly show that distinct distributions of oxygen magnetic moments in the Li0 state. Figure S7 presents scatter plots of the changes in oxygen magnetic moments for all LMO systems. It is evident that structures with higher O porbital contribution tend to exhibit larger oxygen magnetic moments in the Li0 state, and the reverse holds true for systems with lower contribution, demonstrating a strong positive correlation. These findings provide an independent confirmation of oxygen redox participation and further substantiate the reliability of our newly developed descriptor.

For DRX materials, an excessively low O *p*-orbital contribution is unfavorable for providing additional capacity, while an excessively high value will lead to decreased structural stability during redox processes, thereby adversely affecting the cycle life of the material. Therefore, we aim to regulate the O *p*-orbital contribution within a reasonable range in the research on optimizing DRX materials.

Although the preceding section elucidated the regulatory effects of different metal cations on oxygen redox behavior, the impact of an individual metal cation is insufficient to satisfy the rigorous demands of high-performance materials. Prior studies on material optimization have demonstrated that multications synergy can significantly enhance both structural stability and cycling life. The example, Zeng et al. optimized the configurational entropy of LiMn<sub>2</sub>O<sub>4</sub> by introducing five low-valence metal cations, which significantly mitigated structural degradation during prolonged cycling. Therefore, in this section, we aim to regulate the redox behavior and structural stability of DRX-LMO by leveraging the mixed-cation effects induced by multications doping.

We attempted to incorporate metal cations other than Mn as dopants into the DRX-LMO structure. Specifically, in a model with the stoichiometry Li<sub>16</sub>Mn<sub>16</sub>O<sub>32</sub>, 1/4 of the Mn atoms were substituted. The multications doping combinations investigated were: (1) LiMn<sub>0.75</sub>(CrFeCoNi)<sub>0.0625</sub>O<sub>2</sub>; (2)  $L i M n_{0.75} (M g T i C r N b)_{0.0625} O_2;$  (3)  $LiMn_{0.75}(TiCrFeCo)_{0.0625}O_2;$  and (4)  $LiMn_{0.75}(TiVCrCo)_{0.0625}O_2$ . In the following sections, we will use dopant cations to denote the chemical formulas of these structures. The schematic structures are shown in Figure S8. The first three combinations were selected based on cation valence matching, while the fourth combination was designed by excluding cations (Mg, Al, Fe, Ni, Cu) that tended to form O-O dimers in single-cation structures, as well as cations (Zr, Nb, Mo, W) associated with low voltage and large volume changes, thereby retaining only Ti, V, Cr, and Co. In particular, the lower O p-orbital contributions of Ti and V were expected to reduce the overall O p-orbital contribution, thereby mitigating the detrimental effects of O-O dimers formation while maintaining a high voltage.

Here again we used a statistically computational analysis of 20 quasi-random models and included data from the undoped DRX-LMO for comparison (Figures 4 and S9-S10). The results indicate that the distances of O-O in the Li0 state are significantly shortened compared to the Li1 state. The combinations that include elements prone to O-O dimers formation, such as CrFeCoNi, MgTiCrNb, and TiCrFeCo, also exhibit O-O dimers formation. However, the proportion of O-O dimers among all the distances of O-O is nearly an order of magnitude lower compared to the single-cation structures. However, TiVCrCo aligns well with our expectations. By excluding metal cations that induce O-O dimers, this combination successfully avoids the formation of O-O dimers in the Li0 state, resulting in improved structural stability compared to the first three combinations while maintaining a high voltage. Additionally, in CrFeCoNi, the selected cations were found to exhibit high voltage and O porbital contribution in single-cation structures. This trend is also observed in the doped structures, where the structures demonstrate higher voltage and O p-orbital contribution compared to the undoped DRX-LMO. By replacing Ni, an element with relatively high O p-orbital contribution and voltage, in the CrFeCoNi system with Ti, which has lower

values for both metrics, we obtained the TiCrFeCo configuration. As expected, both the O p-orbital contribution and the voltage decreased accordingly. By comparing the magnetic moment data in Table S2 for DRX-LMO, the subtle variations in oxygen magnetic moments shown in Table S3 also reflect the modulation of oxygen participation. These findings confirm that multications doping can effectively regulate oxygen redox behavior in DRX-LMO and validate the feasibility of using single-cation structures analyses to guide the tuning of multications doping strategies. However, due to the relatively high doping concentration and the limitations imposed by the unit cell volume, further adjustments to the dopant ratios were not possible. Moreover, the interaction mechanisms among different metal cations in multications doped systems remain unclear. Therefore, further in-depth investigations are needed to refine our understanding and optimize the design of these materials.

In this study, we performed a systematic first-principles analysis on a series of DRX models to investigate how various metal cations regulate oxygen redox behavior and structural stability in DRX cathodes. We first compared the PDOS of Mn 3d and O 2p in spinel-LMO and DRX-LMO, revealing clear evidence of oxygen participation in redox processes within DRX-LMO. Additionally, we found that the electronic states of oxygen in the O-Li<sub>x</sub>Mn<sub>6-x</sub> structural units vary significantly with both the Li+ content and the number of Li-O-Li configurations, these variations correlate directly with pronounced differences in oxygen redox activity and structural stability. By constructing and analyzing 20 quasi-random configurations, we demonstrated the strong interrelationship between the lattice oxygen redox and transition metal cations during the delithiation process in DRX by analyzing the TM-O and O-O distances, TM and O electronic states, as well as the contribution of oxygen redox. The contrasting electronic structure and local oxygen structure of lattice oxygen in LiXO<sub>2</sub> with different cations suggest two anion redox mechanisms (the RCM and ODM), along with three distinct contribution mechanisms (TM redox-dominated, O redox-dominated, and a balanced contribution from both). Two types of oxygen redox mechanisms and their relevance to the structural and electrochemical behaviors were explained through theoretical investigations of the electronic and magnetic structures. We designed four distinct multication doping systems and examined the electronic and microstructural changes before and after delithiation. Our results demonstrate that the cationic effects of different metals can be used to regulate oxygen redox behavior in manganese-based rock-salt multication systems. These findings represent a significant advance in revealing the relationship between metal cations and oxygen redox activity, offering valuable guidance for the further development of oxygen-active DRX electrode materials. However, regulation of anionic redox alone cannot meet the requirements for future materials. Future studies must adopt a multidimensional evaluation framework that considers reversibility, structural stability, and economic efficiency when assessing DRX material performance.

Computational Methods. All the spin-polarization DFT calculations were implemented in the Vienna Ab initio Simulation Package (VASP) with the projector-augmented method. The electron—ion interaction was described using the projector augmented wave (PAW) method. We employed the generalized gradient approximation (GGA) level of DFT with the Perdew—Burke—Ernzerhof (PBE)

exchange-correlation functional to describe the exchange-correlation effects in this study.  $^{41,43}$  All calculations used a plane wave cutoff energy of 520 eV, with error analysis versus 700 eV presented in the Supporting Information. The total energy convergence criterion for all calculations was set to below  $1.0 \times 10^{-5}$  eV. The Monkhorst-Pack k-point sampling method was carried out for all calculations with  $3 \times 3 \times 3$  kpoint samplings. We expanded the model to a  $2 \times 2 \times 2$ supercell, resulting in a unit cell with 64 atoms. The increased atom count enhances the ability of our model to accurately simulate the inherent disorder of the DRX structure and facilitates subsequent multication doping studies. All calculations were performed with the Hubbard U correction (DFT + U) applied to the transition-metal d orbitals. We selected U values based on previous studies. The U parameters for Ti, V, Cr, Mn, Fe, Co, Ni, Cu, Zr, Nb, Mo, and W ions were set to 4.2, 3.5, 4.0, 3.9, 4.2, 4.0, 6.0, 5.2, 4.0, 4.0, 4.0, and 3.5 eV.  $^{11,44-48}$  Additionally, we discussed the error analysis of our descriptor between the use of DFT+U and HSE06 in the Supporting Information. The calculation workflow was managed by the high-throughput computational platform for the rock-salt LMO battery materials. 10,16

#### ASSOCIATED CONTENT

# **Supporting Information**

The Supporting Information is available free of charge at https://pubs.acs.org/doi/10.1021/acs.jpclett.5c01558.

Model construction and validation, schematic illustrations of single-cation and multication structures, table of lattice parameters, XRD patterns, statistical distributions of X–O and O–O distances, scatter plot of unit-cell volume changes, oxygen-vacancy formation energy formula and results, cation and anion magnetic moments statistics for single-cation and multications systems, calculation methods for O *p*-orbital contributions, O *p*-band center, voltage and volume changes, scatter plot of O *p*-band center distributions for single-cation and multications systems, scatter plot of oxygen magnetic moment variations, error analysis plots for cutoff energy, and HSE06 tests (PDF)

## AUTHOR INFORMATION

### **Corresponding Author**

Bingkai Zhang — School of Chemical Engineering and Light Industry, Guangdong University of Technology, Guangzhou 510006, China; orcid.org/0009-0008-1563-3931; Email: zhangbk@gdut.edu.cn

### Authors

Yanzhao Niu — School of Chemical Engineering and Light Industry, Guangdong University of Technology, Guangzhou 510006, China

Shisheng Wang — School of Chemical Engineering and Light Industry, Guangdong University of Technology, Guangzhou 510006, China

Ruishan Zhang — School of Chemical Engineering and Light Industry, Guangdong University of Technology, Guangzhou 510006, China

Zengzhu Li – School of Chemical Engineering and Light Industry, Guangdong University of Technology, Guangzhou 510006, China Feng Pan — School of Advanced Materials, Peking University, Peking University Shenzhen Graduate School, Shenzhen 518055, China; orcid.org/0000-0002-8216-1339

Wei Deng – School of Big Data Statistics, Guizhou University of Finance and Economics, Guiyang 550025, China

Complete contact information is available at: https://pubs.acs.org/10.1021/acs.jpclett.5c01558

#### Notes

The authors declare no competing financial interest.

#### ACKNOWLEDGMENTS

This research work was supported by the Natural Science Foundation of Guangdong Province (2024A1515030261) and Guizhou Provincial Science and Technology Projects (qiankehejichu [2024] Youth 183, qiankehezhicheng DXGA [2025] yiban014). The computations were performed on the Guangdong University of Technology High Performance Computing Platform.

# REFERENCES

- (1) Manthiram, A. A reflection on lithium-ion battery cathode chemistry. *Nat. Commun.* **2020**, *11* (1), 1550.
- (2) He, W.; Guo, W.; Wu, H.; Lin, L.; Liu, Q.; Han, X.; Xie, Q.; Liu, P.; Zheng, H.; Wang, L.; et al. Challenges and recent advances in high capacity Li-rich cathode materials for high energy density lithium-ion batteries. *Adv. Mater.* **2021**, *33* (50), 2005937.
- (3) Chen, D. C.; Ahn, J.; Chen, G. Y. An Overview of Cation-Disordered Lithium-Excess Rocksalt Cathodes. *ACS Energy Lett.* **2021**, *6* (4), 1358–1376.
- (4) Kang, K.; Meng, Y. S.; Breger, J.; Grey, C. P.; Ceder, G. Electrodes with high power and high capacity for rechargeable lithium batteries. *Science* **2006**, *311* (5763), 977–980.
- (5) Zhang, H.; Gao, X.; Cai, Q.; Zhang, X.; Tian, Y.; Jia, M.; Xie, W.; Du, Y.; Yan, X. Recent progress and perspectives on cation disordered rock-salt material for advanced Li-ion batteries. *J. Mater. Chem. A* **2023**, *11* (16), 8426–8452.
- (6) Seo, D.-H.; Lee, J.; Urban, A.; Malik, R.; Kang, S.; Ceder, G. The structural and chemical origin of the oxygen redox activity in layered and cation-disordered Li-excess cathode materials. *Nat. Chem.* **2016**, 8 (7), 692–697.
- (7) McCalla, E.; Abakumov, A. M.; Saubanère, M.; Foix, D.; Berg, E. J.; Rousse, G.; Doublet, M.-L.; Gonbeau, D.; Novák, P.; Van Tendeloo, G.; et al. Visualization of O–O peroxo-like dimers in high-capacity layered oxides for Li-ion batteries. *Science* **2015**, *350* (6267), 1516–1521.
- (8) Van der Ven, A.; Ceder, G.; et al. Lithium diffusion in layered Li,CoO<sub>2</sub>. Electrochem. Solid-State Lett. **1999**, 3 (7), 301.
- (9) Shi, X.-M.; Watanabe, E.; Okubo, M.; Yamada, A. Does spinel serve as a rigid framework for oxygen redox? *Chem. Mater.* **2020**, 32 (17), 7181–7187.
- (10) Wang, D.; Jiao, Y.; Shi, W.; Pu, B.; Ning, F.; Yi, J.; Ren, Y.; Yu, J.; Li, Y.; Wang, H.; et al. Fundamentals and advances of ligand field theory in understanding structure-electrochemical property relationship of intercalation-type electrode materials for rechargeable batteries. *Prog. Mater. Sci.* **2023**, *133*, 101055.
- (11) Lun, Z.; Ouyang, B.; Kwon, D.-H.; Ha, Y.; Foley, E. E.; Huang, T.-Y.; Cai, Z.; Kim, H.; Balasubramanian, M.; Sun, Y.; et al. Cation-disordered rocksalt-type high-entropy cathodes for Li-ion batteries. *Nat. Mater.* **2021**, 20 (2), 214–221.
- (12) Zhou, K.; Li, Y.; Zheng, S.; Zhang, M.; Zhang, C.; Battaglia, C.; Liu, H.; Wang, K.; Yan, P.; Liu, J.; et al. Tailoring the redox-active transition metal content to enhance cycling stability in cation-disordered rock-salt oxides. *Energy Storage Mater.* **2021**, *43*, 275–283. (13) Pei, Y.; Chen, Q.; Ha, Y.; Su, D.; Zhou, H.; Li, S.; Yao, Z.; Ma, L.; Sanders, K. J.; Sheng, C.; et al. Fluorinated Rocksalt Cathode with

- Ultra-high Active Li Content for Lithium-ion Batteries. Angew. Chem., Int. Ed. 2022, 61 (47), No. e202212471.
- (14) Yu, Z.; Qu, X.; Dou, A.; Su, M.; Liu, Y.; Wu, F. Synthesis and redox mechanism of cation-disordered, rock-salt cathode-material Li—Ni—Ti—Nb—O compounds for a Li-ion battery. *ACS Appl. Mater. Interface* **2019**, *11* (39), 35777—35787.
- (15) Assat, G.; Tarascon, J.-M. Fundamental understanding and practical challenges of anionic redox activity in Li-ion batteries. *Nat. Energy* **2018**, 3 (5), 373–386.
- (16) Shadike, Z.; Zhou, Y.-N.; Chen, L.-L.; Wu, Q.; Yue, J.-L.; Zhang, N.; Yang, X.-Q.; Gu, L.; Liu, X.-S.; Shi, S.-Q.; et al. Antisite occupation induced single anionic redox chemistry and structural stabilization of layered sodium chromium sulfide. *Nat. Commun.* 2017, 8 (1), 566.
- (17) Li, X.; Wang, J.; Zhang, S.; Sun, L.; Zhang, W.; Dang, F.; Seifert, H. J.; Du, Y. Intrinsic Defects in LiMn<sub>2</sub>O<sub>4</sub>: First-Principles Calculations. *ACS Omega* **2021**, *6* (33), 21255–21264.
- (18) Clément, R.; Lun, Z.; Ceder, G. Cation-disordered rocksalt transition metal oxides and oxyfluorides for high energy lithium-ion cathodes. *Energy Environ. Sci.* **2020**, *13* (2), 345–373.
- (19) Goodenough, J. B.; Park, K. S. The Li-Ion Rechargeable Battery: A Perspective. J. Am. Chem. Soc. 2013, 135 (4), 1167–1176. (20) Goodenough, J. B.; Kim, Y. Challenges for Rechargeable Li
- Batteries. Chem. Mater. 2010, 22 (3), 587–603.
- (21) Guin, S.; Ghosh, S.; Sarkar, S. S.; Maitra, U. Reviewing Li-Rich Disordered Rocksalts as Next-Generation High-Energy Cathode Material. *Chem. Mater.* **2024**, *36* (21), 10421–10450.
- (22) Lee, J.; Kitchaev, D. A.; Kwon, D.-H.; Lee, C.-W.; Papp, J. K.; Liu, Y.-S.; Lun, Z.; Clément, R. J.; Shi, T.; McCloskey, B. D.; et al. Reversible Mn<sup>2+</sup>/Mn<sup>4+</sup> double redox in lithium-excess cathode materials. *Nature* **2018**, *556* (7700), 185–190.
- (23) Zhong, P.; Cai, Z.; Zhang, Y.; Giovine, R.; Ouyang, B.; Zeng, G.; Chen, Y.; Clément, R.; Lun, Z.; Ceder, G. Increasing capacity in disordered rocksalt cathodes by Mg doping. *Chem. Mater.* **2020**, 32 (24), 10728–10736.
- (24) Dianat, A.; Seriani, N.; Bobeth, M.; Cuniberti, G. Effects of Aldoping on the properties of Li-Mn-Ni-O cathode materials for Li-ion batteries: an ab initio study. *J. Mater. Chem. A* **2013**, *1* (32), 9273–9280
- (25) Tang, W.; Li, A.; Zhou, G.; Chen, Z.; Yang, Z.; Su, J.; Zhang, W. Interfaces. Structural stabilization of cation-disordered rock-salt cathode materials: coupling between a high-ratio inactive Ti<sup>4+</sup> cation and a Mn<sup>2+</sup>/Mn<sup>4+</sup> two-electron redox pair. *ACS Applied Materials* **2022**, *14* (34), 38865–38874.
- (26) Sallard, S.; Billaud, J.; Sheptyakov, D.; Novák, P.; Villevieille, C. Cr-doped Li-rich nickel cobalt manganese oxide as a positive electrode material in Li-ion batteries to enhance cycling stability. *ACS Appl. Energy Mater.* **2020**, 3 (9), 8646–8657.
- (27) Yoon, W.-S.; Balasubramanian, M.; Chung, K. Y.; Yang, X.-Q.; McBreen, J.; Grey, C. P.; Fischer, D. A. Investigation of the charge compensation mechanism on the electrochemically Li-Ion deintercalated Li<sub>1-x</sub>Co<sub>1/3</sub>Ni<sub>1/3</sub>Mn<sub>1/3</sub>O<sub>2</sub> electrode system by combination of soft and hard X-ray absorption spectroscopy. *J. Am. Chem. Soc.* **2005**, *127* (49), 17479–17487.
- (28) Petersburg, C. F.; Li, Z.; Chernova, N. A.; Whittingham, M. S.; Alamgir, F. M. Oxygen and transition metal involvement in the charge compensation mechanism of LiNi<sub>1/3</sub>Mn<sub>1/3</sub>Co<sub>1/3</sub>O<sub>2</sub>cathodes. *J. Mater. Chem.* **2012**, 22 (37), 19993–20000.
- (29) Luo, K.; Roberts, M. R.; Hao, R.; Guerrini, N.; Pickup, D. M.; Liu, Y.-S.; Edström, K.; Guo, J.; Chadwick, A. V.; Duda, L. C.; et al. Charge-compensation in 3*d*-transition-metal-oxide intercalation cathodes through the generation of localized electron holes on oxygen. *Nat. Chem.* **2016**, 8 (7), 684–691.
- (30) Hong, J.; Gent, W. E.; Xiao, P.; Lim, K.; Seo, D.-H.; Wu, J.; Csernica, P. M.; Takacs, C. J.; Nordlund, D.; Sun, C.-J.; et al. Metaloxygen decoordination stabilizes anion redox in Li-rich oxides. *Nat. Mater.* **2019**, *18* (3), 256–265.
- (31) Zhang, S.; Chen, H.; Chen, J.; Yin, S.; Mei, Y.; Ni, L.; Di, A.; Deng, W.; Zou, G.; Hou, H.; et al. Mitigating the Jahn-Teller

- distortion driven by the spin-orbit coupling of lithium manganate cathode. *J. Energy Chem.* **2022**, *72*, *379*–*387*.
- (32) Yu, J.; Wang, D.; Wang, G.; Cui, Y.; Shi, S. Breaking the electronic conductivity bottleneck of manganese oxide family for high-power fluorinated graphite composite cathode by ligand-field high-dimensional constraining strategy. *Adv. Mater.* **2023**, 35 (8), 2209210.
- (33) Massaro, A.; Muñoz-García, A. B.; Prosini, P. P.; Gerbaldi, C.; Pavone, M. Unveiling Oxygen Redox Activity in P2-Type Na<sub>x</sub>Ni<sub>0.25</sub>Mn<sub>0.68</sub>O<sub>2</sub> High-Energy Cathode for Na-Ion Batteries. *ACS Energy Lett.* **2021**, *6* (7), 2470–2480.
- (34) House, R. A.; Rees, G. J.; McColl, K.; Marie, J.-J.; Garcia-Fernandez, M.; Nag, A.; Zhou, K.-J.; Cassidy, S.; Morgan, B. J.; Saiful Islam, M.; Bruce, P. G. Delocalized electron holes on oxygen in a battery cathode. *Nat. Energy* **2023**, *8* (4), 351–360.
- (35) Vergnet, J.; Saubanère, M.; Doublet, M.-L.; Tarascon, J.-M. The Structural Stability of P2-Layered Na-Based Electrodes during Anionic Redox. *Joule* **2020**, *4* (2), 420–434.
- (36) Hammer, B.; Nørskov, J. K. Electronic factors determining the reactivity of metal surfaces. *Surf. Sci.* **1995**, 343 (3), 211–220.
- (37) Li, X.; Zhang, W.; Lv, K.; Liu, J.; Bayaguud, A. Research progress on high-entropy oxides as advanced anode, cathode, and solid-electrolyte materials for lithium-ion batteries. *J. Power Sources* **2024**, *620*, 235259.
- (38) Huang, C.; Luo, J.; Mansley, Z. R.; Kingan, A.; Campos, A. R.; Wang, Z.; Bernardez, E. J. M.; Pace, A.; Ma, L.; Ehrlich, S. N.; et al. Manganese-rich high entropy oxides for lithium-ion batteries: materials design approaches to address voltage fade. *J. Mater. Chem. A* **2024**, *12* (38), 26253–26265.
- (39) Zeng, W.; Xia, F.; Wang, J.; Yang, J.; Peng, H.; Shu, W.; Li, Q.; Wang, H.; Wang, G.; Mu, S.; et al. Entropy-increased LiMn<sub>2</sub>O<sub>4</sub>-based positive electrodes for fast-charging lithium metal batteries. *Nat. Commun.* **2024**, *15* (1), 7371.
- (40) Kresse, G.; Furthmüller, J. Efficiency of ab-initio total energy calculations for metals and semiconductors using a plane-wave basis set. *Comput. Mater. Sci.* **1996**, 6 (1), 15–50.
- (41) Kresse, G.; Furthmüller, J. Efficient iterative schemes for ab *initio* total-energy calculations using a plane-wave basis set. *Phys. Rev.* B **1996**, 54 (16), 11169.
- (42) Blöchl, P. E. Projector augmented-wave method. *Phys. Rev. B* **1994**, *50* (24), 17953.
- (43) Perdew, J. P.; Chevary, J. A.; Vosko, S. H.; Jackson, K. A.; Pederson, M. R.; Singh, D. J.; Fiolhais, C. Atoms, molecules, solids, and surfaces: Applications of the generalized gradient approximation for exchange and correlation. *Phys. Rev. B* **1992**, *46* (11), 6671.
- (44) Cai, Z.; Ouyang, B.; Hau, H.-M.; Chen, T.; Giovine, R.; Koirala, K. P.; Li, L.; Ji, H.; Ha, Y.; Sun, Y.; et al. In situ formed partially disordered phases as earth-abundant Mn-rich cathode materials. *Nat. Energy* **2024**, *9* (1), 27–36.
- (45) Das, H.; Urban, A.; Huang, W.; Ceder, G. First-principles simulation of the (Li-Ni-vacancy) O phase diagram and its relevance for the surface phases in Ni-rich Li-ion cathode materials. *Chem. Mater.* **2017**, 29 (18), 7840–7851.
- (46) Jain, A.; Hautier, G.; Moore, C. J.; Ong, S. P.; Fischer, C. C.; Mueller, T.; Persson, K. A.; Ceder, G. A high-throughput infrastructure for density functional theory calculations. *Comput. Mater. Sci.* **2011**, *50* (8), 2295–2310.
- (47) Morgan, B. J.; Carrasco, J.; Teobaldi, G. Variation in surface energy and reduction drive of a metal oxide lithium-ion anode with stoichiometry: a DFT study of lithium titanate spinel surfaces. *J. Mater. Chem. A* **2016**, *4* (43), 17180–17192.
- (48) Sai Gautam, G.; Carter, E. A. Evaluating transition metal oxides within DFT-SCAN and SCAN+U frameworks for solar thermochemical applications. *Phys. Rev. Mater.* **2018**, 2 (9), 095401.